Wear Tribo-Performances of Laser Cladding Colmonoy-6 and Stellite-6 Micron Layers on Stainless Steel 304 Using Yb:YAG Disk Laser

N. Jeyaprakash[1,2] · Che-Hua Yang[1,2] · Sheng-Po Tseng[2]

Abstract

Stainless steel material has been widely used in aeronautical, chemical and nuclear industries due to good corrosion resistance. However, the material has less hardness and wear resistance. In this study, two various depositions namely Colmonoy-6 and Stellite-6 have produced on 304 Stainless steel. Besides, the coating was examined to reveal their metallurgical, mechanical and tribological properties. In addition, wear mechanism, wear debris and roughness averages were studied. The outcomes indicate that both coatings show with dendrite structure due to rapid cooling rates. Hardness of the clad surface has improved than substrate material. The results of friction coefficient of specimen with Colmonoy-6 is lower than that of specimens Stellite-6 and substrate. Also, wear resistance of Colmonoy-6 has increased 49 times than substrate sample, which reveals that Colmonoy-6 laser cladding plays role on wear resistance. Adhesive and abrasive are the major wear mechanisms in the present study.

Keywords Stainless steel 304 · Laser cladding · XRD · Microstructure · Hardness · Wear performance · Wear debris · Roughness

1 Introduction

Stainless steels (SS) is most commonly used material in aeronautical, chemical and nuclear power industries for their excellent corrosion resistance. However, they have relatively less hardness and wear resistance. Hence, the material SS usually need for surface modification or treatment to improve their hardness and wear properties [1]. Modern techniques of surface engineering allow the various types of composite and complex coatings. The coatings such as plasma, thermal spraying and laser remelting, pre-placed coating or diffusion layers were reported frequently in literature [2–7]. The laser technique, which is based on the principle of laser material surface manufacturing and/or modification has widely recognized as a promising technique than other surface modification techniques, due to its higher cooling rates (10^{-3}–10^{-8} Ks^{-1}) and flexibility [8, 9]. The several microstructural changes can be attained with unique properties which do not reach by conventional methods. Laser treatment comprises surface hardening, quenching, melting, alloying and cladding [10–16]. Among those techniques, laser cladding is a hardfacing technique which can produce a laser source to heat the surface. Further, it can feed the powders on the substrate material with low dilution and specific quality which is properly fused on the base material. Therefore, the laser cladding offers researchers and engineers to optimize the material properties for the existing materials and to develop new ones [17].

Hardfacing of alloy powders has been for a long practice to enhance the tribological properties of metals [18]. In recent years, iron, nickel and cobalt based hard facing alloys are used in many applications due to its excellent wear properties, high hardness and thermal resistance. Among these, Colmonoy-6 and Stellite-6 powders are attracted more as a wear resistance coating. Ramasubbu et al. [19] investigated the dilution effect of Colmonoy-6 on 316 SS metal using

✉ N. Jeyaprakash
prakash84gct@gmail.com; prakash@ntut.edu.tw

Che-Hua Yang
chyang@ntut.edu.tw

Sheng-Po Tseng
tseng3392@gmail.com

1 Centre of Mass Customization Additive Manufacture, National Taipei University of Technology, Taipei 10608, Taiwan, R.O.C.

2 Institute of Manufacturing Technology, National Taipei University of Technology, Taipei 10608, Taiwan, R.O.C.

GTAW (Gas tungsten arc welding). The results indicated that boride fraction was increased from 5 to 8% with a reduction in dilution. Fernandes et al. [20] have examined the oxidation behavior of nickel based hardfacing coating on gray cast iron using PTA (plasma transferred arc) method.

Kumar et al. [21] have studied the wear behavior of TIG (Tungsten inert gas) deposited Ni–Cr–B coating on 316LN SS. The outcome has shown that improved wear resistance and friction coefficient was observed on Ni–Cr–B coatings. Singh et al. [22] have studied the effect of Stellite-6 cladding on erosion and cavitation erosion. Results showed that Stellite-6 cladding has improved the erosion and cavitation resistance on SS. Ferozhkhan et al. [23] have studied the wear resistance of Stellite-6 coating using PTA. The outcomes showed that the wear resistance was improved through PTA hard facing and useful in valve application at high temperature. Based on the literature, there are other methods such as TIG, PTA and GTAW was adopted to deposit the hard powders on the base material. There is no comparison of metallurgical, mechanical and wear study of Colmonoy-6 and Stellite-6 deposition on 304 SS using Yb:YAG disk laser. In this study, metallurgical, mechanical and tribological performance

of both coatings have studied. Besides, wear mechanisms and roughness of worn out surfaces have analysed.

2 Experimental Procedure

2.1 Samples and Laser Cladding

A Ni-based Colmonoy-6 and Co-based Stellite-6 powders were used as coating material with the particle size of 53–155 μm (Fig. 1a–d). Stainless steel 304 was used as the base material (substrate) with the dimensions of $30 \times 30 \times 30$ mm. The base material was sand blasted to
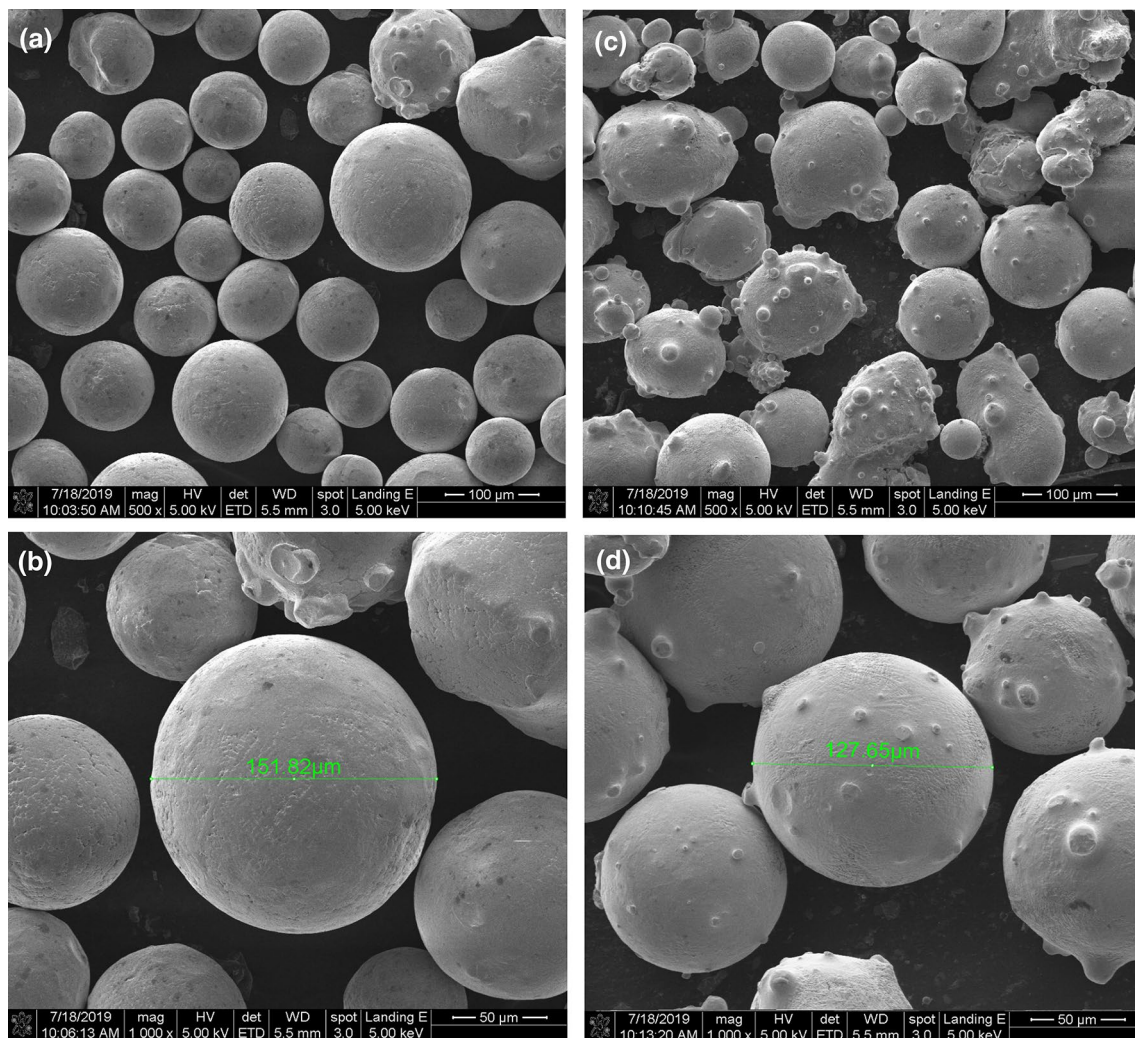

Fig. 1 SEM picture of as-received alloy powders **a**, **b** Colmonoy-6, **c**, **d** Stellite-6

Table 1 Chemical composition of powders and substrate

Materials	Elements composition (wt%)								
	Ni	Co	Cr	Fe	W	B	Si	C	Mn
Colmonoy-6	REM	0.07	14.67	3.67	–	3.41	4.53	0.81	–
Stellite-6	0.65	REM	28.27	0.84	4.41	–	1.20	1.28	0.11
Stainless steel 304	9.77	–	19.22	REM	–	–	0.79	0.1	1.98

Table 2 Laser cladding parameters

Power	1000 W
Scanning speed	600 mm/min
Feed rate	7 g/min
Spot size	3.2 mm
Stand-off	15 mm
Overlapping	50%
Powder carrier gas (argon)	6 SD@1 bar
Shielding gas (argon)	25 lpm
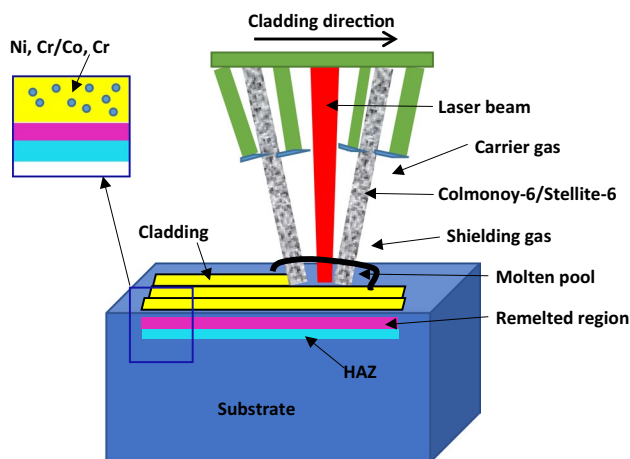
Fig. 2 Schematic picture of laser cladding process

obtain a surface roughness of 7 microns which improves the adhesiveness of coatings. Then, the prepared specimens were cleaned with acetone and dried completely with hot air. Table 1 indicates the chemical compositions of selected materials. A high power Yb:YAG disk laser was used to clad the selected powders on substrate material. The wavelength of laser beam was about 1030 nm and circular shape beam mode was applied. A deposition 300 μm thickness of Colmonoy-6 and Stellite-6 alloy powders were separately exposed to the laser source. The process parameters such as power (W), scanning speed (mm/min) and feed rate (g/min) was varied and found optimized laser clad parameter based on defect free and good bonding of the coating. The optimized laser parameter and schematic picture of laser cladding process is shown in Table 2 and Fig. 2, respectively.

2.2 Test Samples Preparation and Characterization

The proper specimens for experimental work were cut from the cladded blocks through resin-bonded alumina blades with applying the constant lubricants. The cladding specimens were cross sectioned to analyse the structure and hardness. Also, the coated specimen was cut into pin shape with dimensions of $6 \times 6 \times 30$ mm for the wear test. The cross sectioned specimens were polished with various emery sheet with suitable chemicals to reveal the structure. The powder particle size and coating cross-section were examined using optical microscopy (OM) (Olympus) and FE-SEM (JEOL-JSM-7610F) equipped with energy dispersive spectroscopy (EDS). The produced coating thickness (300 μm) were measured and confirmed with Optical microscopy. The coating cross-sections were shown in Fig. 3. X-ray diffraction study has conducted on both hard powders and clad surfaces using Cu-Kα energy produced at 40 kV and 40 Ma. Hardness test were performed to analyse the hardness variation between cladding and base material regions. As per ASTM G99-05 standards, dry sliding wear test was performed [24]. Figure 4 shows schematic picture of pin-on-disc apparatus. Load, velocity and distance were selected as input parameters for wear study. The specimen weight was measured after and before the test to calculate the material loss. Beside, wear debris, roughness and mechanism of worn surfaces was analyzed.

3 Results and Discussion

3.1 Phase Structure Analysis

In order to identify the formed phase structure on the cladded surface, X-ray analysis was conducted on top of the surfaces. X-ray analysis of Colmonoy-6 cladding surface is shown in Fig. 5a. The most dominant peak is fcc γ-Ni due to solid solution of nickel elements [25]. The other peaks namely $(Ni, Fe)_3 B$ and Cr_5B_3 were present on laser processed surface [26]. The combination of borides and nickel formed the interdendritic structure and the blacky black phase is CrB (Fig. 6b). The primary solidification was helped to form the chromium carbide phase. In Colmonoy alloy series, formation of borides and carbides over laser cladding was reported by Li et al. [27] and Conde et al.
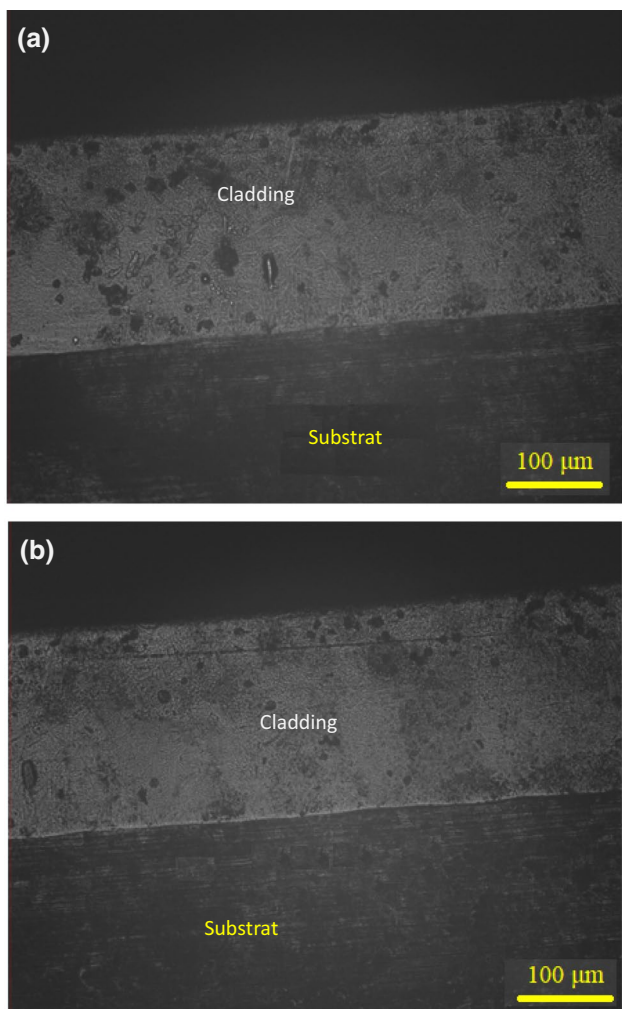
Fig. 3 Cross sectional optical images of cladding **a** Colmonoy-6 and **b** Stellite-6

[28]. X-ray result of Stellite-6 cladding surface was shown in Fig. 5b. From the XRD peaks, it was noticed that γ-Co peak was most dominant than other peaks. Also, the metastable phases such as Cr_7C_3 and $Cr_{23}C_6$ were noticed during the X-ray analysis [29]. High amount of carbide phases such as $M_{23}C_6$ and M_7C_3 which is fundamentally chromium carbides and M_6C peak also observed as refractory element by combined molybdenum and tungsten [30, 31]. The observed carbides were agreeing with Co–C–Cr phase diagram. After laser coating, the formed phases are lowered and broadened because of grain changes as shown in XRD spectra. The fast cooling rate can change the grain structures on the formed layer.

3.2 Microstructure Analysis

FE-SEM was used to study the structure of cross sectioned Colmonoy-6 and Stellite-6 coatings. No defects were observed from the examined coating cross sections. In Colmonoy-6 coating, it can be observed the dendrite structure towards the buildup direction. The EDS examination has revealed the dendrite to be γ-nickel and which also have other elements such as Si, Cr and Fe. The γ-nickel and boride phases shows as lighter region and darker regions, respectively [32]. The showed borides are mostly as Ni-borides. However, Fe and Cr elements was present as shown in elemental analyses [33]. In initial track, Fe elements favored to form Cr borides with more fraction of iron. The noticed various percentage of chromium borides and Ni–B–Si with iron elements compositions can change the solidification path of Colmonoy alloy. The fusion line increases as Fe element decreases and eutectic structure can be noticed. The same observations were found by Zhang et al. [26], in their

Fig. 4 Schematic picture of Pin-on-disc setup
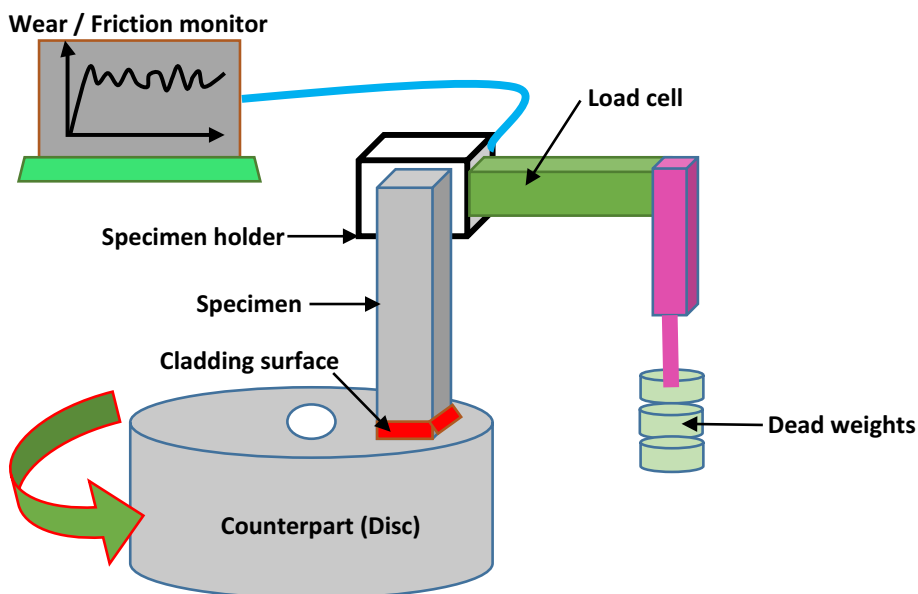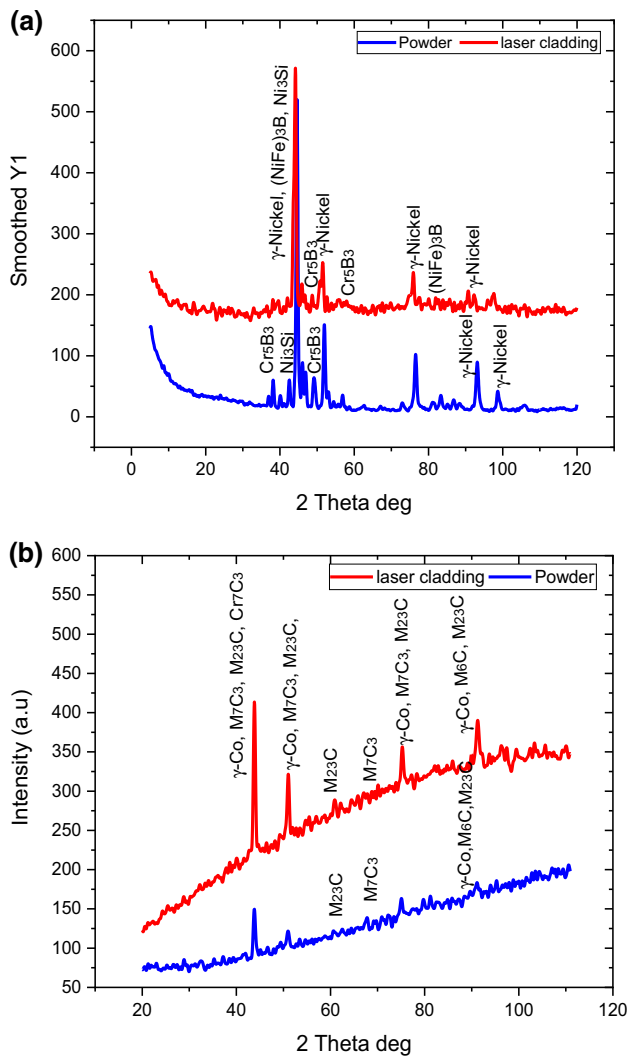
Fig. 5 XRD analysis of powders and cladding surface **a** Colmonoy-6 and **b** Stellite-6

investigation of NiCrSiBC powders on SS316L through CO$_2$ laser cladding. Figure 6 shows OM, FESEM images and EDS spectrum of Colmonoy-6 cladding. The optimized parameters produced the finer coating without defects. Because of solidification rate, it can be noticed various structure on the cladding region. The variations in structure from base material to top of the clad shown in Fig. 6a. The microstructure shows the differences from the edge to centre point of the laser track length at the cladding surface. Temperature gradient (G) is linearly associated to cooling rate (R). Therefore, decreasing the ratio of G/R, the structure like cellular to dendrite were observed in the present study. In interface region, the base material acts like heat sink with less duration of solidification (t) and higher temperature gradient (TG). The planer recrystallization arrangement can be
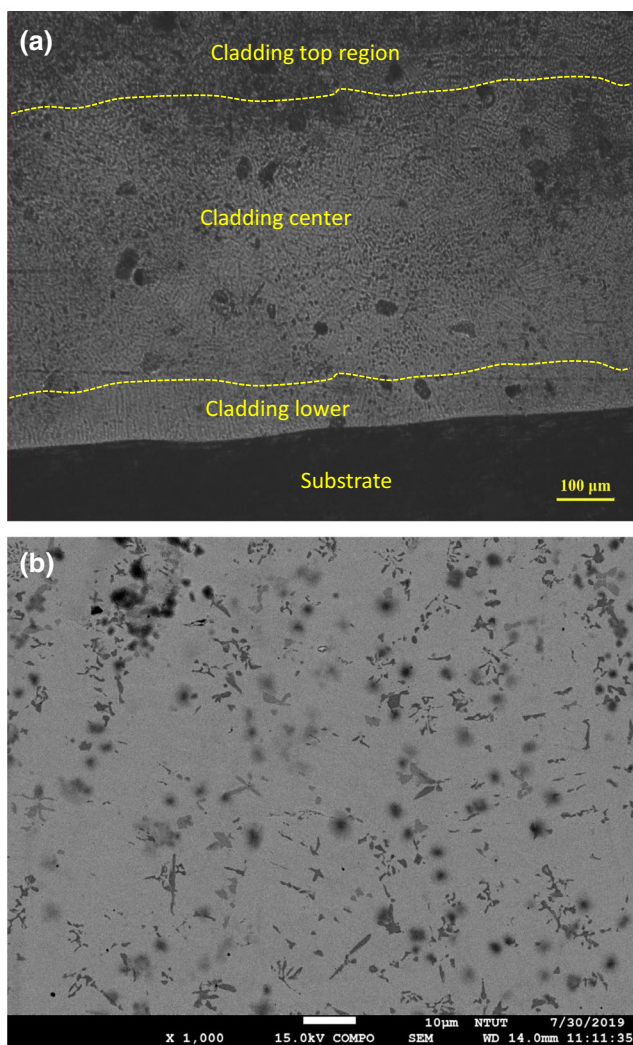
noticed due to higher ration of temperature gradient and time [34]. The various structure was observed on the cladding surfaces while middle region of the coating shows with dendritic and different phases. Besides, interdendritic eutectic structure can be noticed on the cladding. Reaction between carbon and oxygen elements may cause the porosity during laser treatment. In the present study, argon gases were used to avoid oxidation process during treatment. Hence, the measurement of pores is not considered in the present study.

FE-SEM results of Stellite-6 cladding show that fine dendrite structure. This is due to rapidly solidified microstructure in which a lesser volume of liquid metal was cooled by a sink of large substrate ensuing into higher cooling rates. The structure of the high power laser clad with Stellite-6 is a hypoeutectic microstructure having chromium rich interdendrites and cobalt rich dendrites [22]. Based on phase diagram of Co–Cr–W, cobalt rich phase was created in dendrite form from the liquid state. In liquid state, cooling rate is high and producing small primary and secondary dendrites. The formed dendrites indicate a super saturated solid solution of cobalt–chromium through precise orientation and interdendrite along grain boundary as displayed in Fig. 7. In the beginning, dendrites were formed as columnar, cellular and changed to dendritic structure due to temperature difference during solidification process. Higher laser source melts the substrate and powder particle to create a molten pool. Then, the laser beam moves to another region, the partially melted powders starts to solidify and formed the homogeneous interdendrite structure. The structure of Stellite-6 was divided into three different zones such as base metal, heat affected zone and clad zone. The heat affected zone have mixed elements of Stellite-6 and stainless steel. The carbon is responsible for wear protection through developing the carbides with the metals in Co–Cr by developing M$_6$C and M$_7$C$_3$ carbides. The EDS examination was carried out on Stellite-6 cross section in three different spots namely A, B and C. A—near the coating top surface; B—center of the coating cross section; C—near the substrate and coating interface to study the dilution of Fe element in the produced coating and confirm the bonding between substrate and coating. The analyzed all the three points has confirmed the Stellite-6 alloy elements composition. The percentage of Fe element was not more than 2.1% in all the three analyzed spots. The dendrite microstructure can be observed in inside every individual splats. The observed structure was quite similar on the entire coating thickness. Figure 7 shows OM, FESEM images and EDS spectrum of Stellite-6 cladding. EDS examination in the eutectic structure (Figs. 6d, 7d) showed with elements of Ni, Cr, Co, Si, W, Fe which represents chances of formation of eutectic carbides.
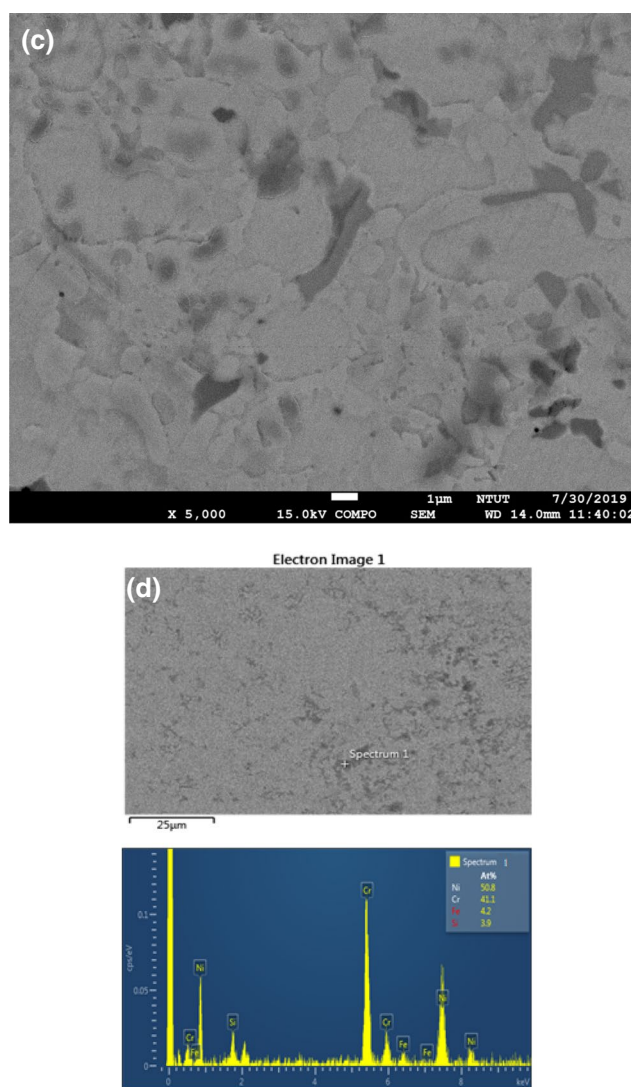
3.3 Microhardness Analysis

The microhardness testing was performed on the cross section of laser clad samples. This investigation was made to evaluate the hardness variations on laser clad samples and substrate material. Figure 8(a) shows the schematic picture of microhardness indentation in different region, (b) cross sectional SEM picture with coating thickness and (c) measured hardness profile across the cladding depth. The average microhardness of stainless steel was 227 $HV_{0.3}$. After laser cladding with Colmonoy-6 and Stellite-6 alloy powders, the hardness was enhanced up to 2.5 (566.8 $HV_{0.3}$) and 2 times (487.52 $HV_{0.3}$), respectively. Also, temperature effect and subsequent microstructure modifications may be the reason for hardness variations [34]. This was verified practically

Fig. 7 Cross sectional OM picture shows the three different regions; ▶ cladding region, interface and substrate **a**, FE-SEM picture of Stellite-6 cladded interface region **b**, cladded center region with higher magnification **c**, EDS analysis were performed in three different regions to identify the base metal dilution **d**

that while a hard alloy powders were fused or/bonded on the smoother surface, the hardness of the bonded or fused layer was improved [36]. Similarly, Li et al. [37] were observed the same results in fusion of tough alloy particle into smoother surface. It was due to the dendrite and/inter-dendrite structure that restricted the plastic distortion created by the hardness indenter. Therefore, dendrite/interdendrite structure have shown the greater strengthening effect on the laser clad region. In Colmonoy-6 cladding, higher hardness
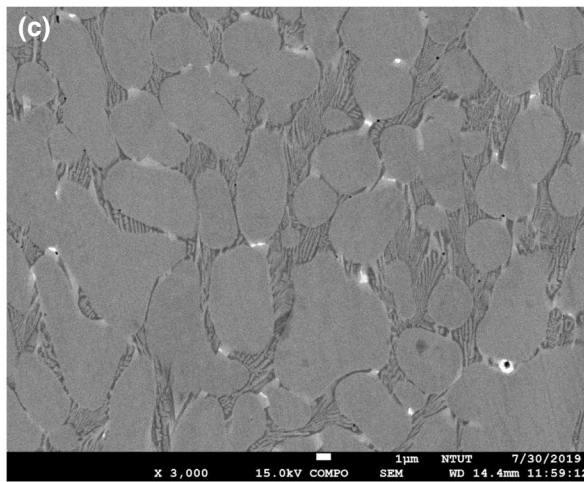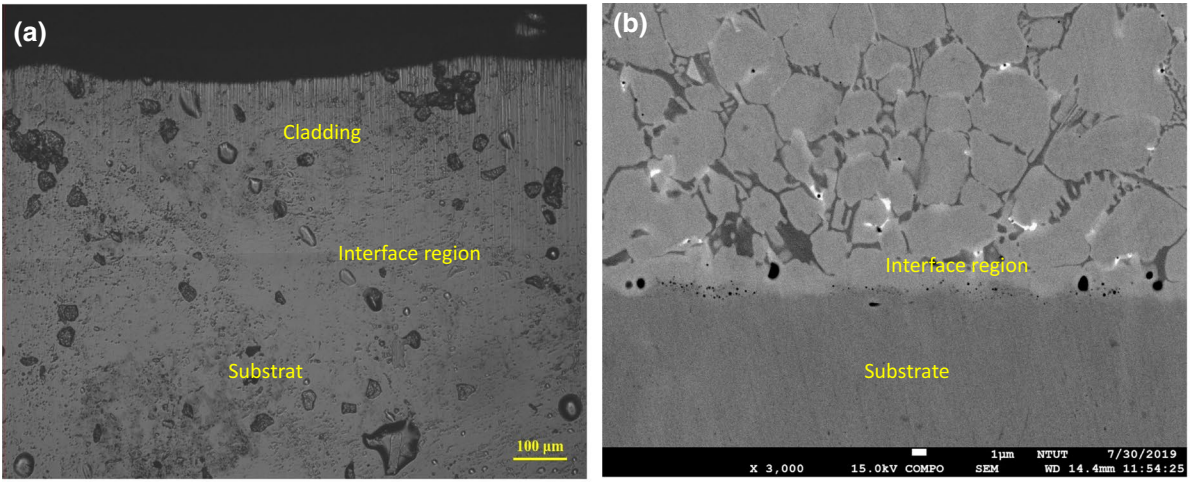
Fig. 6 Cross sectional OM picture shows the three different regions; cladding lower region, center region and top region **a**, FE-SEM picture of Colmonoy-6 cladded region with lesser magnification **b**, with higher magnification **c** with EDS analysis **d**
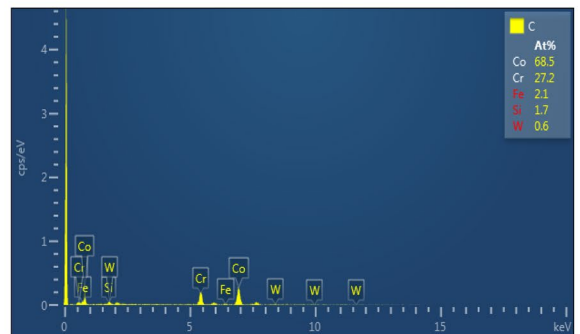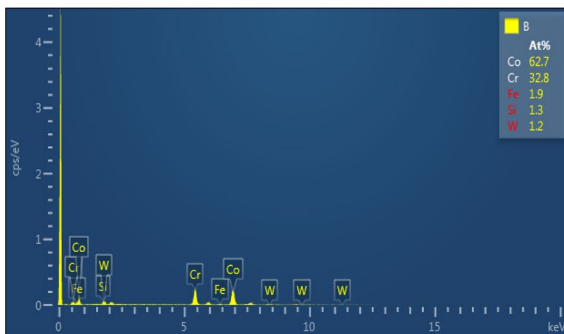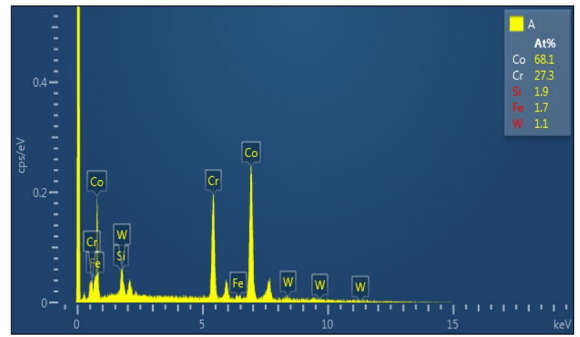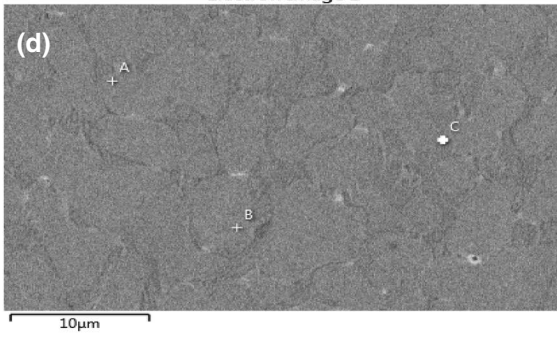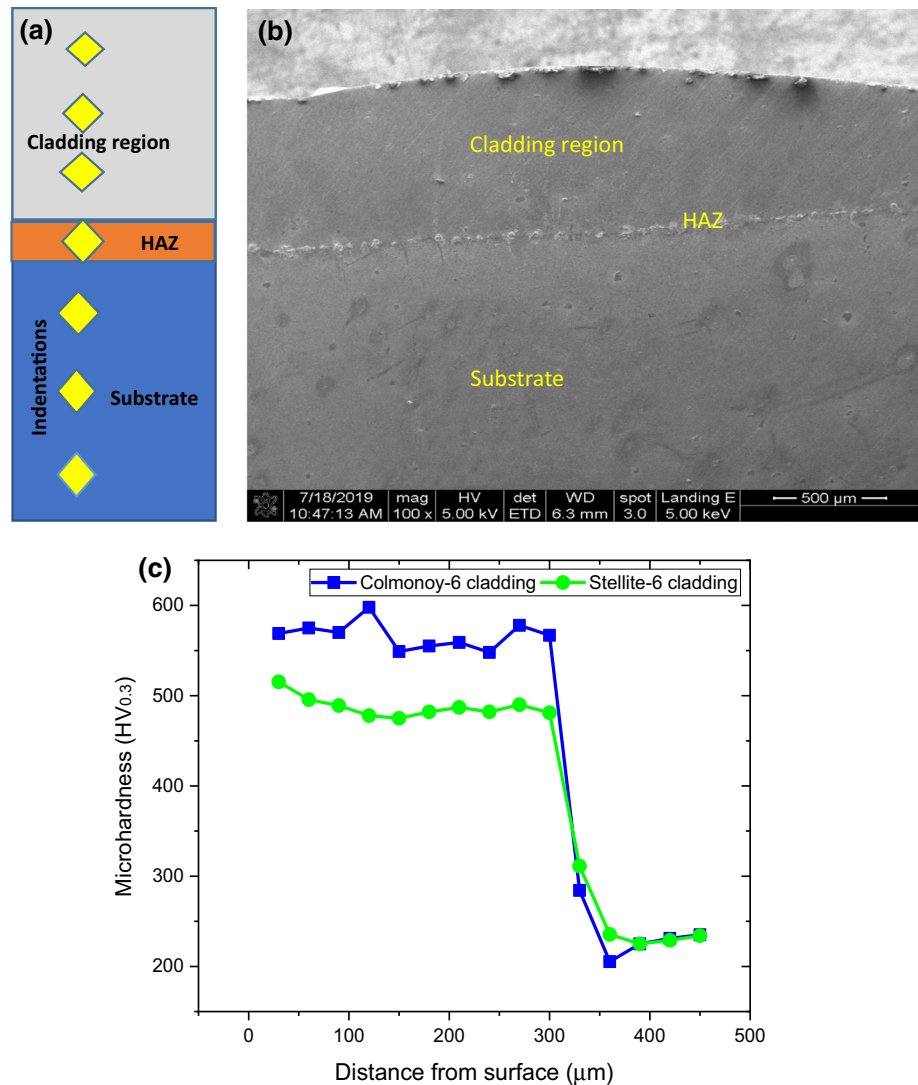
Fig. 8 **a** Schematic picture of microhardness indentation in three different regions; cladding region, heat affected zone and substrate, **b** cross sectional SEM picture with showing three different regions, **c** microhardness profile of laser cladded cross section
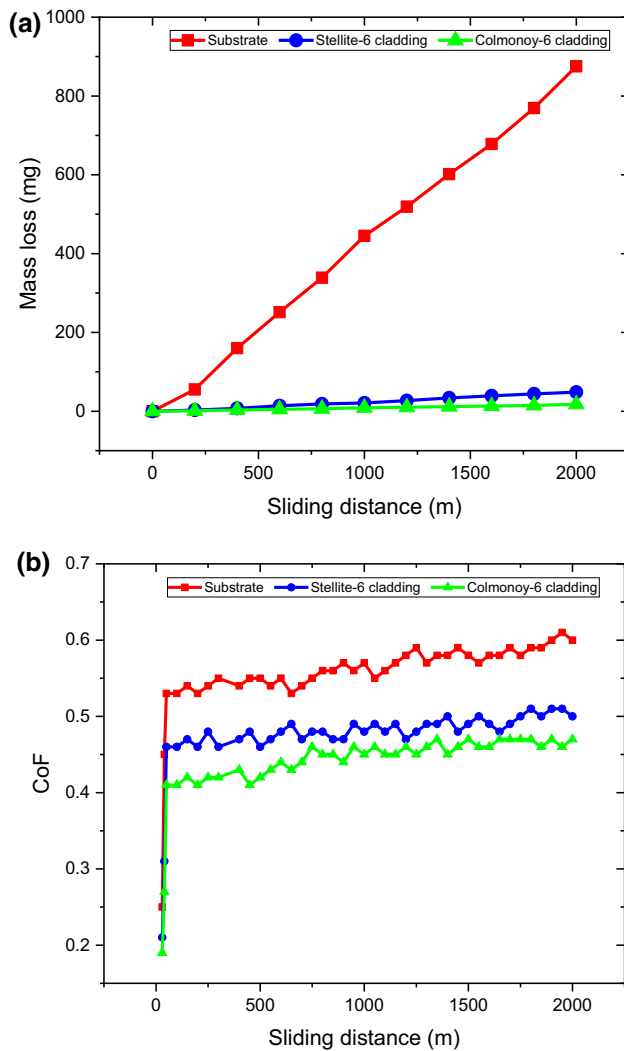

was observed due to the presence of boride and carbide phases which can dilute the hard particles to base material surface. Furthermore, the residual stress, which is produced by rapid heating and cooling through laser clad, might be reason to the enhancement of hardness. All the clad layers were achieved more hardness than substrate material due to the formation of solid solutions of alloying elements. The measured hardness profile shows nearly constant on treated area because of formation of homogeneous structure. In Stellite, microhardness of dark carbide-containing region is more than that of lighter regions. Cr based dark region also was higher which shows an increase of hardness of those regions. It can be noted that the hardness was increases from interface region to surface. This may be attributed due to the finer grain size of particles and diffusion of Fe atoms to the interface. The earlier investigation on Stellite-6 with respect to microstructure and hardness are revealed that formation of quasi-martensitic structure was increased the hardness

on the weld metal adjacent to bulk metal. The laser source reaches the substrate and alloy powders, also it affects seriously steel material due to its melting point. During this time, the steel material mixed with coating material and shows little deviations.

3.4 Wear and Friction Behavior

Dry sliding tribo-test phenomenon is generally a complex procedure, which includes various tribo parameters such as atmosphere temperature, physical properties and loading conditions etc. [38]. The dry sliding wear study results were presented in Fig. 9a, in which the total mass loss was compared with distance in meter. Based on the achieved outcomes, it can be observed that the mass loss of the laser clad samples (γ-nickel and γ-cobalt) was less than substrate material. The material loss on substrate was about ~875.31 mg which is more than ~17.71 mg (Colmonoy-6) and ~48.32 mg

Fig. 9 **a** Mass loss, **b** CoF of substrate and laser cladded samples

However, it remains almost constant with increase in sliding distance. Reducing wear amount with medium load results from increases in contact area, helps to minimize the contact pressure. As an outcome, rate of metal removal by rolling and grooving effects promoted through abrasive particle is reduced. In the start condition, laser clad samples increased the weight loss and after reach some sliding distance shows stable condition due to formation of oxide layer through sliding surface [39]. The main reason to form the oxide layer is increases in surface temperature. However, oxide layers can be noticed at lower temperatures. This can be predicted that rubbing between two surfaces, increases the temperature at the contact surfaces. Therefore, the heat sources are locally increases and oxide layers were formed [29].

Those formed oxides get entrapped between two contact surfaces or it can be detached in the form of wear debris thus developing a layer to protect the Colmonoy-6/Stellite-6 surfaces and improve the wear resistance [40]. In other hand, the formed oxide layer on the contact surface protects further from the wear. The depth of the wear and wear track were noticeable on the Stellite-6 cladded sample while compared with Colmonoy-6 sample. The dilution of various layers on Stellite-6 has less influence on wear properties at the top surface rather close to fusion boundaries and co-efficient of friction as reported. The frictional coefficient (CoF) of substrate and laser cladding specimens was presented against total sliding distance as shown in Fig. 9b. The CoF of substrate material was less in the initial condition and later increased from ~0.53 to 0.61 then maintains constant. The stable increase in CoF after the small drop in the beginning is due to the contact of disc and pin that would progress into self-mating stage, making clean contact area between disc and pin. So, friction force has increased, the same did for CoF also. The friction coefficient of laser cladding Colmonoy-6 and Stellite-6 samples shows nearly 0.41–0.47 and 0.46–0.51, respectively and values are almost constant. From achieved results, it can be observed that the substrate CoF was more than that of laser treated specimens. The frictional heat was produced over contacting surfaces and causes increase in temperature resultant the oxide formation. This oxide layer with less shear energy resulted lower CoF [41].

3.5 Wear Mechanism

Figure 10a–f shows the FE-SEM of worn out surfaces. The used tribological parameters are 50 N load, 1 m/s sliding speed and 2000 m sliding distance. The mass loss of the base material was higher compared with laser processed specimens. The examined base material shows with deep grooves on the surface which shows severe deformation and lesser wear resistance. The micro abrasion is purely based on volumetric fraction, microstructure, strengthen phase distribution and morphology. Besides, base material hardness
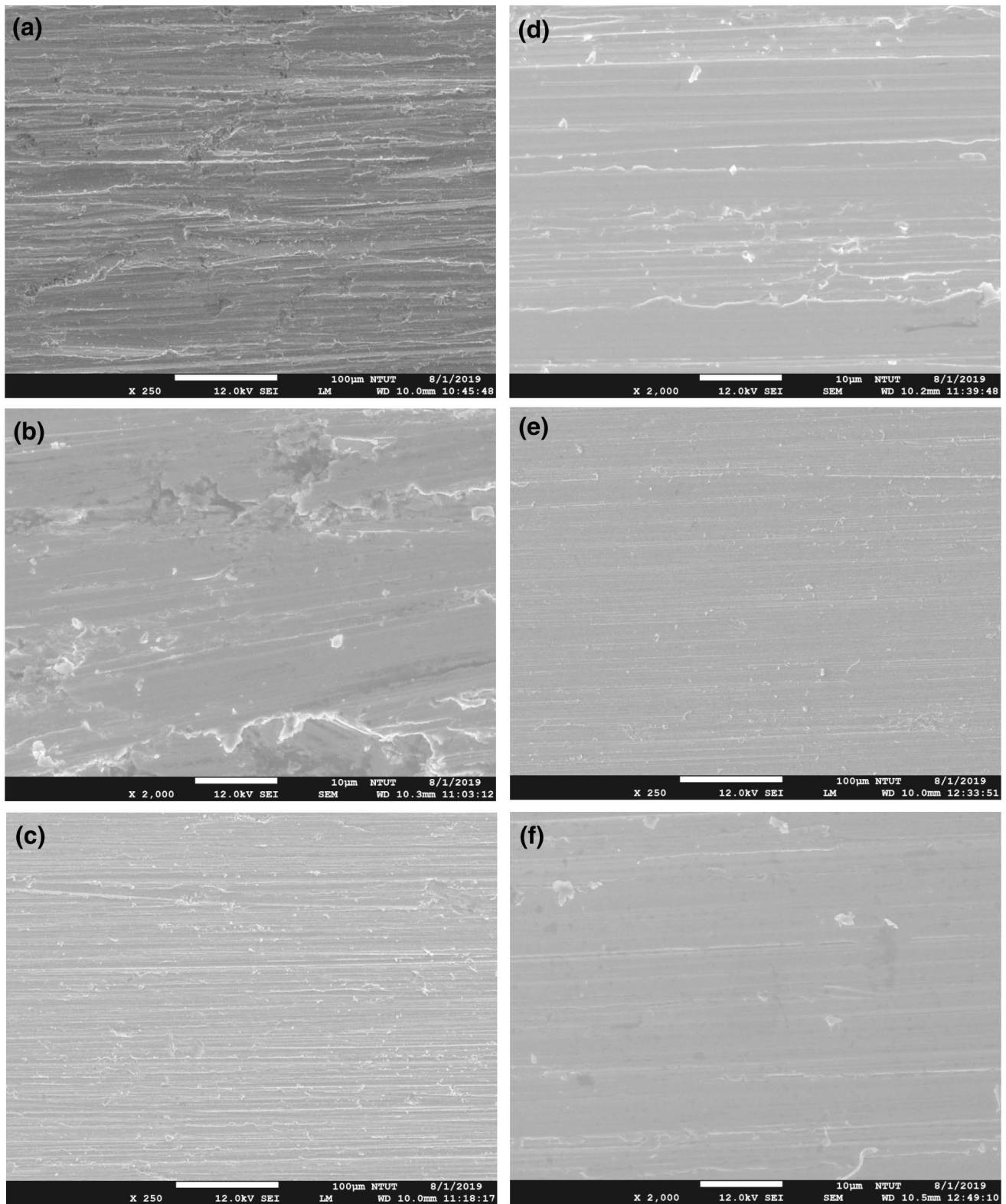
(Stellite-6) for 2000 m rotating distance. The hard alloy powders have improved the substrate hardness after laser cladding. The formed interdendritic structure with the combination of nickel and boride improved the wear properties. CrB mixed nickel alloy shows more load carrying capacity and avoid the mechanical damages from the possible wear scratches. The creation of hydrodynamic film between cladding and counterpart surfaces while higher rotational speed, which helps to make more gap in rotating surfaces. Similarly, the combination of chromium and cobalt was improved the hardness and toughness of the coating. Because Co elements were considered as a tough material and Cr offers moderate hardness. The Co element act as a binder and was responsible for the densification process through spreading, wetting and formation of agglomerates in liquid sintering. Furthermore, the weight loss of base metal is increases while increasing the sliding distance. The wear amount reduces with raising sliding speed (disc) and load.
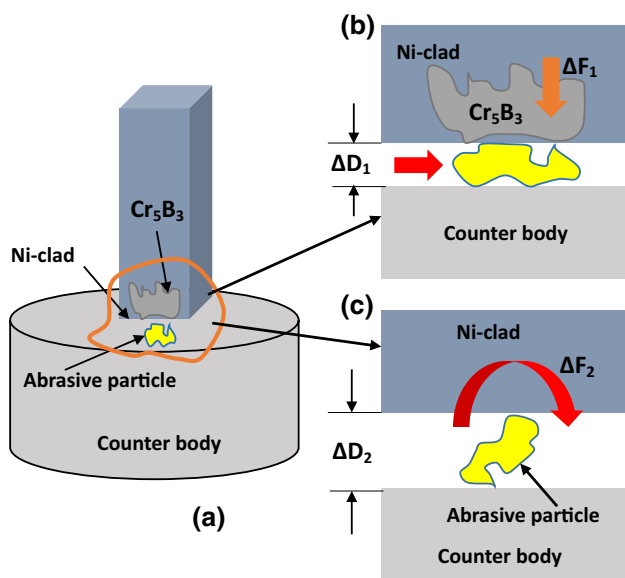
Fig. 10 FE-SEM micrograph of worn out surfaces, **a**, **b** Substrate, **c**, **d** Stellite-6 and **e**, **f** Colmonoy-6 cladded samples

Fig. 11 Schematic illustration of the adhesive wear at the interface matrix/boride **a** before sliding, **b** the cladded pin sliding over the counter part with high contact pressure, **c** after sliding with piled-up material (adhesive)
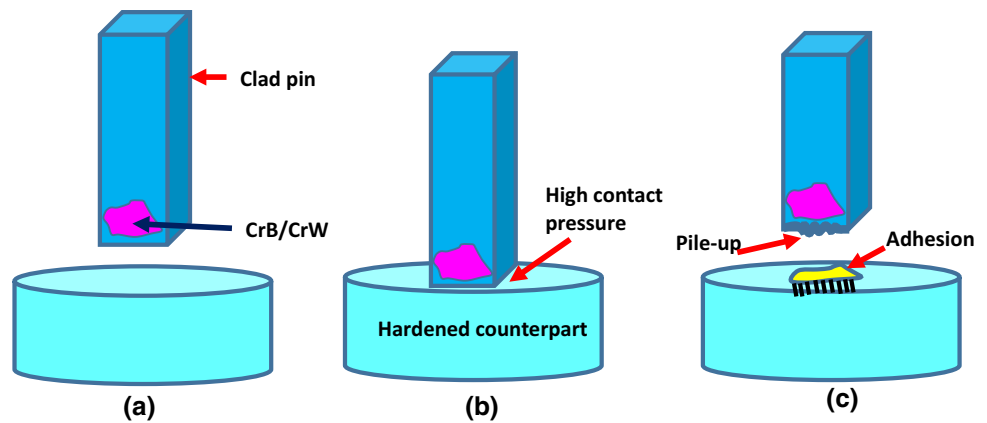
is heavily affects the abrasion resistance. Hence, substrate material causes less wear resistance than cladding specimens. However, laser cladding samples deformed less while compared to substrate and enhanced the wear resistance. The wear track of laser cladding samples shows in Fig. 9c–f, it can be noticed that the wear track is smooth on the cladding sample. From the cladding surface, the bright area indicates the locations where material was detached from the cladding layers. Also, the laser cladding surface got scratched less compared to substrate material. The cladding surfaces exhibited less material loss due to the hardfacing alloy powders Colmonoy-6 and Stellite-6. When cladding surface meets the counterpart, the extended area of the disc hard-pressed the cladding surface. As an outcome, adhesion and scuff was occurred [42], which is stuck the movement between pin and disc. However, the frictional force and material loss
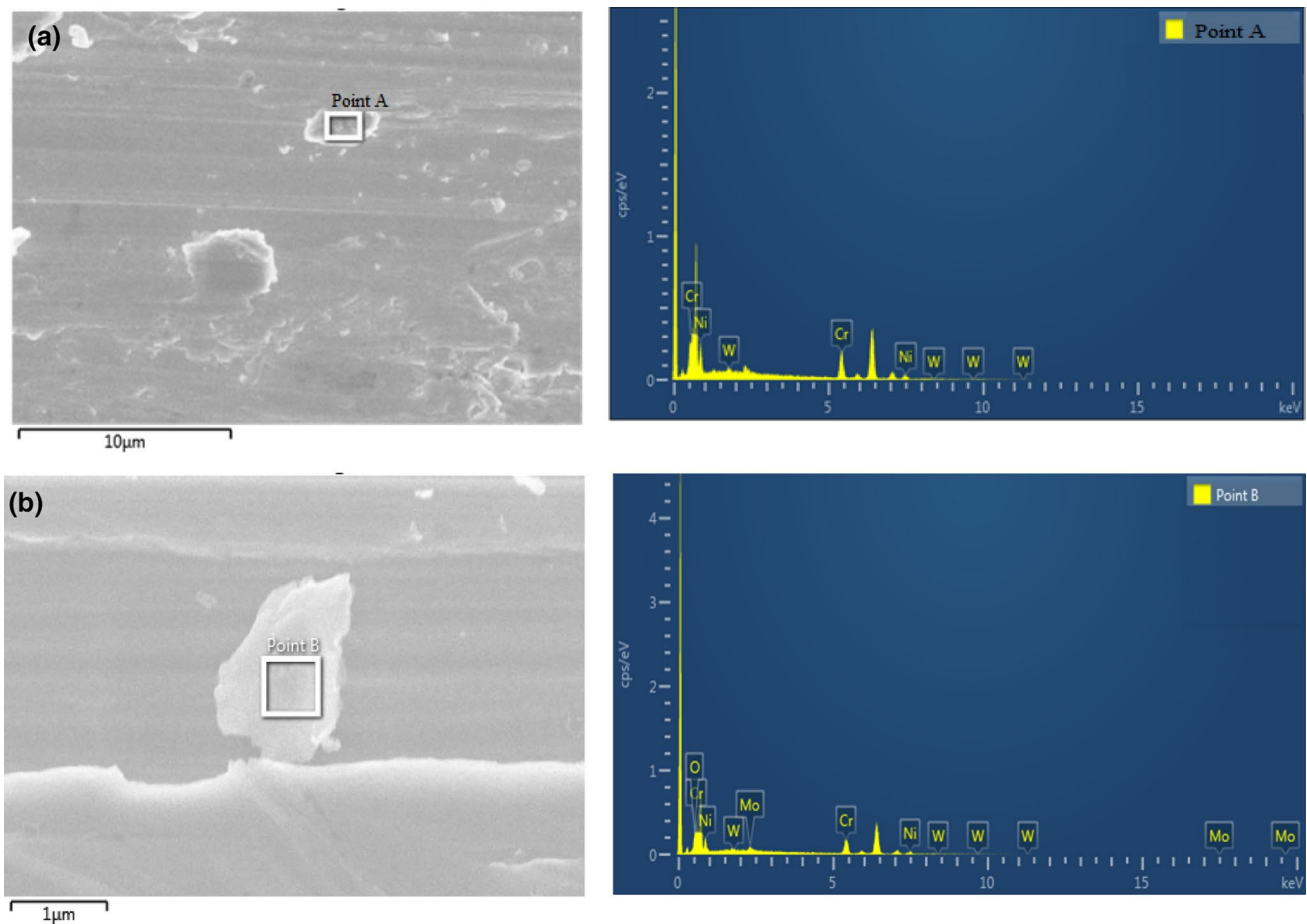
were minimum. The produced wear track shows less depth and material pile-up were less. The finer scratches can be noticed from the cladding samples and this can be indicating the less material loss on laser cladding samples. The reason for this less material loss due to formation of dendrite structure which shows higher hardness of cladding samples [9]. The enhanced wear properties are assumed to be the combined solution of the even distribution of hard phase, grain refining effect and good bonding between matrix and hardfacing alloys. The harder Colmonoy-6 and Stellite-6 cladding surfaces has enhanced the strength against abrasion and improved the wear properties. The observed major wear mechanism is abrasives and adhesives. The straight interaction between pin and disc might have produced the abrasive particle. Those particles may stay on the disc surfaces and further acts to promote the abrasive wear. The harder counterpart produces a track on the treated surface after sliding some distance [43]. Further, while pin slides on the disc, the ball tend to pull and press the debris on the wear track. Both abrasive and adhesive mechanisms have happened more or less simultaneously. The cladding surface sliding on the counter part was exposed to adhesive wear whereas, at the front of it, a pile-up of debris is being pushed causing abrasive wear.

Figure 11 explains the step by step procedure of adhesive wear. As the treated regions touches and sliding on the counterpart surface, the harder elements (Cr, B and W) increases the pressure at the contact point of matrix and harder elements. Besides, matrix can be deformed and adhered to the counter body [44]. Hence, the material loss was increased due to gathered removed material. The treated surface continuously sliding on the disc surface and pulls out the material from the surface causes adhesive wear. Therefore, this irregular damaged surfaces and debris causes abrasive wear. In addition, on laser cladding surface the principal mechanism is grooving in both strengthening phase and matrix. Hence, the noticed variations in the wear mechanism with cladding microstructure can be associated to the creation of large floret-shape chromium borides in Colmonoy

Fig. 12 Schematic illustration of the interaction between Cr_5B_3 phases and abrasive particles, **a** before sliding, **b** the cladding surface sliding over the abrasive particle with D_1 distance, **c** the cladding surface sliding over the abrasive particle with D_2 distance

Fig. 13 FE-SEM picture of wear debris and EDS analysis **a** Stellite-6 and **b** Colmonoy-6

cladding. Generally, these types of large size chromium borides (Cr_5B_3) works as load bearing areas. The enhancement of wear resistance on formation of floret shape Cr_5B_3 [45] and it is illustrated in Fig. 12. On the floret shape Cr_5B_3, the abrasive particles experience a lesser distance (ΔD_1) between both surfaces with relatively higher load (ΔF_1). At this moment, the matrix is higher worn compared to hard borides (Cr_5B_3). Now, the abrasive particles were move into translational motion and forming grooves on the Cr_5B_3 boride surface. But, when the abrasive particles move along with coating region (Ni), the gap between two surfaces will increase ($\Delta D_2 > \Delta D_1$) and the applied load becomes lesser (ΔF_2). In this stage, the surface (Ni clad) gets higher significant wear when compared to chromium boride (Cr_5B_3), and allowing rotational movements which can cause microrolling on the nickel based coating surface [46].

*Normal applied force* ($\Delta F1$) *> Normal applied force* ($\Delta F2$)

Initial distance between surface ($\Delta D1$) *>*

Final distance between surface ($\Delta D2$)

where F—applied force; D—distance between surfaces.

3.6 Wear Debris and Roughness Analyses

The wear debris of Colmonoy-6 and Stellite-6 were analyzed using FE-SEM and reported that the abrasive and adhesive wear are the superior wear mechanism in the present investigation. Also, some delamination wear has been observed. The formed debris may be from the bulges on the cladded sample during sliding condition. The sheets like shape or thick flakes were formed as wear debris because of delamination type of wear. The abrasive type wear also has been reported due to the presence of elements such as Ni, Cr, Co and W or the combination of various types of wear mechanisms. The hard particles may act as sharp cutting edges which will plough the material from the contact area and then it may have scratched or/damaged while reaches some few thousand meters, causing abrasive wear. Figure 13 shows the wear debris picture with EDS analysis. Worn-out pin surfaces were shown in Fig. 14. It was noticed that the substrate surface shows a higher roughness of ~ 4.8 µm due
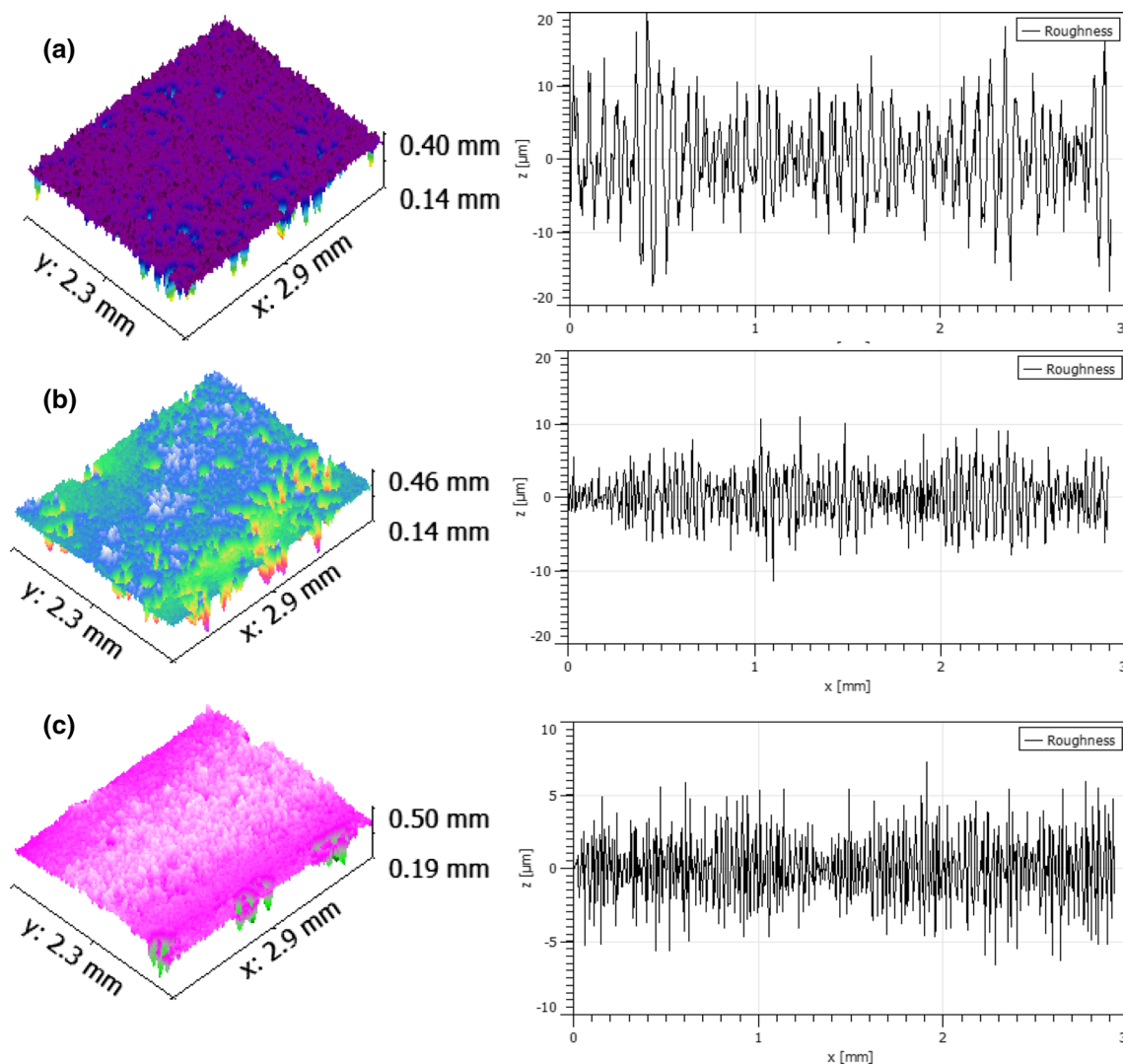
Fig. 14 Worn out pin roughness averages of **a** Substrate, **b** Stellite-6 and **c** Colmonoy-6

to lower hardness and higher material loss. The laser cladding worn-out surfaces exhibit a lower roughness of ~2.5 µm (Stellite-6) and ~1.8 µm (Colmonoy-6), respectively. This may be due to improved material hardness and reduced wear rate. The laser cladding samples exhibited ~2.3 and ~3 times roughness reduction than substrate sample.

4 Conclusion

The comparison of microstructure and wear resistance of Colmonoy-6 and Stellite-6 coatings has been made on Stainless steel 304 substrate. It was observed that the produced cladding with different alloy powders was influenced the phase composition, microstructure, microhardness and wear resistance. Based on the experimental results the following conclusion were drawn.

- The microstructure of the Colmonoy-6 and Stellite-6 cladding consisted of carbides embedded in a Ni-rich and Co-rich solid solution with dendritic structure, respectively. Primary phases were formed on Colmonoy-6 and Stellite-6 is mixing of γ-Ni with borides and γ-Co lamellar eutectic phases $M_{23}C_6$, M_6C, Cr_7C_3, respectively.
- Microhardness profile indicating that the hardness was increased about 2 to 2.5 times with deposition of Stellite-6 and Colmonoy-6. This may be the presence of finer grain size at the cladding surface while comparing to that of interface.
- Colmonoy-6 cladded SS-304 surface showed lower wear rate than stellite-6 cladded SS-304 surface. The combination of borides and nickels formed the interdendrite structure and improved the wear resistance of the coating. The CoF of laser cladded Colmonoy-6 and Stellite-6

samples shows nearly 0.41–0.47 and 0.46–0.51, respectively and the values are almost constant.

- Adhesive and abrasives are most dominant wear mechanism. Also, some plate-like wear debris was observed which indicates delamination wear.
- The laser cladding samples exhibited ~ 2.3 and ~ 3 times roughness reduction than substrate sample due to improved hardness and lower wear rate.
- In general, wear properties enhancement is assumed to be the combined solution of the even distribution of hard phase, grain refining effect and good bonding between matrix and hardfacing alloys.

References

1. M.K. Kumar, R. Saravanan, R. Sellamuthu, V. Narayanan, Mater. Today: Proc. **5**, 7571 (2018)
2. M. Afzal, M. Ajmal, A. Nusair Khan, A. Hussain, R. Akhter, Opt. Laser Technol. **56**, 202 (2014)
3. J.R. Davis, *Surface Engineering for Corrosion and Wear Resistance* (ASM International, Cleveland, 2001)
4. A. Bartkowska, A. Pertek, M. Jankowiak, K. Jozwiak, Arch. Metall. Mater. **57**, 211 (2012)
5. J.R. Davis, *Handbook of Thermal Spray Technology* (ASM International, Cleveland, 2004)
6. W.M. Steen, J. Mazumder, *Laser Material Processing* (Springer, Berlin, 2010)
7. J.C. Ion, *Laser Processing of Engineering Materials: Principles, Procedure and Industrial Application* (Butterworth-Heinemann, Oxford, 2005)
8. E. Jonda, Z. Brytan, K. Labisz, A. Drygała, Arch. Metall. Mater. **61**, 1309 (2016)
9. N. Jeyaprakash, M. Duraiselvam, R. Raju, Arch. Metall. Mater. **63**, 1303 (2018)
10. Q.B. Liu, H. Liu, J. Mater. Process. Technol. **88**, 77 (1999)
11. W. Tarasiuk, A.I. Gordienko, A.T. Wolocko, J. Piwnik, B. Szczucka-Lasota, Arch. Metall. Mater. **60**, 2939 (2015)
12. B.S. Yilbas, S.Z. Shuja, S.M.A. Khan, A. Aleem, Appl. Surf. Sci. **255**, 9396 (2009)
13. W.L. Xu, T.M. Yue, H.C. Man, C.P. Chan, Surf. Coat. Technol. **200**, 5077 (2006)
14. J.H. Yao, L. Wang, Q. Zhang, F.Z. Kong, C.H. Lou, Z.J. Chen, Opt. Laser Technol. **40**, 838 (2008)
15. B.G. Guo, J.S. Zhou, S.T. Zhang, H.H. Zhou, Y.P. Pu, J.M. Chen, Mater. Sci. Eng. A **480**, 404 (2008)
16. A.H. Wang, X.L. Zhang, X.F. Zhang, X.Y. Qiao, H.G. Xu, C.S. Xie, Mater. Sci. Eng. A **475**, 312 (2008)
17. Yuxin Li, Su Keqiang, Peikang Bai, Wu Liyun, Bin Liu, Su Hongwen, Du Wenbo, Met. Mater. Int. **25**, 1366 (2019)
18. Hsuan-Han Lai, Chih-Chun Hsieh, Chi-Ming Lin, Wu Weite, Met. Mater. Int. **22**, 101 (2016)
19. V. Ramasubbu, G. Chakraborty, S.K. Albert, A.K. Bhaduri, Mater. Sci. Technol. **27**, 573 (2011)
20. F. Fernandes, A. Cavaleiro, A. Loureiro, Surf. Coat. Technol. **207**, 196 (2012)
21. H. Kumar, V. Ramakrishnan, S.K. Albert, A.K. Bhaduri, K.K. Ray, J. Nucl. Mater. **495**, 431 (2017)
22. R. Singh, D. Kumar, S.K. Mishra, S.K. Tiwari, Surf. Coat. Technol. **251**, 87 (2014)
23. M.M. Ferozhkhan, M. Duraiselvam, R. Ravibharath, Procedia Technol. **25**, 1305 (2016)
24. Standard Test Method for Wear Testing with a Pin-on-Disk Apparatus, ASTM Standard, 2010, G: 99-05
25. L.C. Lim, Q. Ming, Z.D. Chen, Surf. Coat. Technol. **106**, 183 (1998)
26. H. Zhang, Y. Shia, M. Kutsuna, G.J. Xu, Nucl. Eng. Des. **240**, 2691 (2010)
27. Q. Li, D. Zhang, T. Lei, Ch. Chen, W. Chen, Surf. Coat. Technol. **137**, 122 (2001)
28. A. Conde, F. Zubiri, J. de Damborenea, Mater. Sci. Eng. A **334**, 233 (2002)
29. A. Gholipour, M. Shamanian, F. Ashrafizadeh, J. Alloys Compd. **509**, 4905 (2011)
30. G.R. Mirshekari, S. Daee, S.F. Bonabi, M.R. Tavakoli, A. Shafyei, M. Safaei, Surf. Interfaces **9**, 79 (2017)
31. M. Laridjani, A. Amadeh, H. Kashani, Mater. Sci. Technol. **26**, 1184 (2010)
32. C.P. Paul, A. Jain, P. Ganesh, J. Negi, A.K. Nath, Opt. Lasers Eng. **44**, 1096 (2006)
33. L.C. Lim, Q. Ming, Z.D. Chen, Surf. Coat. Technol. **106**, 183 (1998)
34. C. Navas, R. Colaco, J. de Damborenea, R. Vilar, Surf. Coat. Technol. **200**, 6854 (2006)
35. N. Jeyaprakash, C.-H. Yang, M. Duraiselvam, G. Prabu, Results Phys. **12**, 1610 (2019)
36. N. Jeyaprakash, M. Duraiselvam, S.V. Aditya, Surf. Rev. Lett. **26**, 1950009 (2019)
37. P. Li, L.Y. Wu, Y.M. Guiong, X. Liu, Mater. Sci. Eng. A **546**, 146 (2012)
38. V.E. Buchanan, P.H. Shipway, D.G. McCartney, Wear **263**, 99 (2007)
39. D. Kesavan, M. Kamaraj, Surf. Coat. Technol. **204**, 4034 (2010)
40. G. Chakraborty, N. Kumar, C.R. Das, S.K. Albert, A.K. Bhaduri, S. Dash, A.K. Tyagi, Surf. Coat. Technol. **244**, 180 (2014)
41. R. Ahmed, O. Ali, N.H. Faisal, N.M. Al-Anazi, S. Al-Mutairi, F.L. Toma et al., Wear **322**, 133 (2015)
42. K. Velmanirajan, A.S.A. Thaheer, R. Narayanasamy, C.A. Basha, Mater. Des. **41**, 239 (2012)
43. Y. Birol, Wear **269**, 664 (2010)
44. L.J. da Silva, A.S.C.M. D'Oliveira, Wear **350**, 130 (2016)
45. L.J. da Silva, C.J. Scheuer, A.S.C.M. D'Oliveira, Wear **428**, 387 (2019)
46. R.C. Cozza, J. Mater. Res. Technol. **3**, 191 (2014)